ISBN: 978-3-95450-236-3 ISSN: 2673-5350 doi:10.18429/JACoW-IBIC2023-TUP027

MICROBUNCHING OF THERMIONIC CATHODE RF GUN BEAMS IN THE ADVANCED PHOTON SOURCE S-BAND LINAC *

J. Dooling†, A. Brill, N. Kuklev, I. Lobach, A. Lumpkin, N. Sereno, Y. Sun
Argonne National Laboratory, Lemont, IL, USA

Abstract

We report on measurements of beams from thermionic cathode (TC) rf guns in the Advanced Photon Source S-Band Linac. These measurements include the macropulse out of both new and existing TC guns as well as the observation of microbunching within the micropulses of these beams. A gun chopper limits the macropulse FWHM duration to the 10 ns range. Our objectives were to analyse the new TC gun and investigate microbunching within a TC-rf-gun-generated beam. Our diagnostics elucidated longitudinal beam structures from the ns to the fs time scales. Coherent transition radiation (CTR) interferometers responding to far-infrared wavelengths were employed after each compression stage to provide the autocorrelations of the sub-ps micropulse durations. The first compression stage is an alpha magnet and the second a chicane. A CCD camera was used to image the beam via optical transition radiation from an Al screen at the end of the linac and also employed to measure coherent optical transition radiation (COTR) in the visible range. The COTR diagnostic observations, implying microbunching on a fs time scale, are presented and compared with a longitudinal space-charge impedance model.

INTRODUCTION

The injection system of the Advanced Photon Source (APS) has relied on thermionic cathode (TC) rf guns as electron-beam sources since 2001 [1]. This will continue to be the case for the APS Upgrade with the multi-bend achromatic magnet lattice installation in the 6 GeV storage ring currently in progress [2]. There are two such S-Band TC rf guns installed in the linac so that one is a "hot" spare. We report the basic testing of the beams from new generation TC rf guns manufactured by RadiaBeam Technologies (RBT) [3] in terms of the ≈10 ns long macropulse composed of micropulses with an S-Band repetition frequency (2856 MHz). We obtained basic macropulse data for a newly installed RBT gun to comparison with one of a set of three TC rf guns purchased from AET Associates (AET) in 2001. The AET guns have been the primary electron source for the APS since that time.

Our interest was to measure the charge of each micropulse within the macropulse structure from the chopper-gated [4], TC-rf gun [5–7]. The extraction of charge from the TC rf gun involves high-power rf applied to the cathode; thus, the extracted charge comes in a series of micropulses. With the macropulse temporal distribution, we can then determine the charge per micropulse. Only the AET gun was employed for the bunch compression experiment discussed below.

In the APS linac, the micropulse duration after the alpha magnet is sub-ps. After further compression in the chicane, longitudinal space charge (LSC) induced microbunching within the micropulses generates coherent optical transition radiation (COTR) when striking the downstream intercepting Al screen. The COTR (visible wavelengths, fs temporal scale) was transported out of the tunnel to a CCD camera, and the images were recorded. We present a comparison of the observed COTR enhancements with the predictions of a LSC-impedance model.

EXPERIMENTAL DESCRIPTION

A schematic of the linac with components relevant for the present discussion is presented in Fig. 1. Compression is provided by the alpha magnet at the end of the gun beam line and the L3 chicane after the first four accelerating structures in L2. Coherent Transition Radiation far-infrared (CTR FIR) interferometers, positioned in the L2 section (L2:CTR) and after the chicance (L3:CTR), provide longitudinal pulse length data [8]. Average current is monitored immediately after the gun and macropulse charge is measured after the alpha magnet in the linac beamline. Optical transition radiation (OTR) and COTR are generated by an Al screen (S5:OTR, as shown in Fig. 1) when struck by the electron beam. An optical transport line guides the light to a camera system outside of the tunnel.

A block diagram of the macropulse duration measurement is presented in Fig. 2. Raw beam signals from the four button pickups are input to 20 dB directional couplers (Mini-Circuits ZGDC20-33HP+). The coupled signals ("c") are combined to form the sum output (Mini-Circuits ZN4PD-642W-S+) which is fed into one channel of a fast oscilloscope with 50 Ω input impedance. The main, uncoupled signals continue on to the analog conditioning electronics associated with the rest of the S-band linac BPMs [9–11]. Because of capacitive coupling, the DC component of the macropulse is not present. Alternatively, the summing unit can be bypassed to provide coupled input to the oscilloscope from all four of the BPM channels. Four channel input allows for observation of beam position within the macropulse. The BPM rf signals are digitally undersampled by the oscilloscope's analog-to-digital converter following the discussion in Ref. [12].

A new 1.5-cell, TC rf gun developed by RBT was installed at the RG1 location in the linac during the December 2022-January 2023 APS maintenance period. We wished to measure the macropulse waveform of this gun to compare with that of the operating TC gun. Further tests with the RBT

* Work supported by the U.S. D.O.E., Office of Science, Office of Basic Energy Sciences, under contract number DE-AC02- 06CH11357.
† dooling@aps.anl.gov

ISBN: 978-3-95450-236-3 ISSN: 2673-5350 doi:10.18429/JACoW-IBIC2023-TUP027

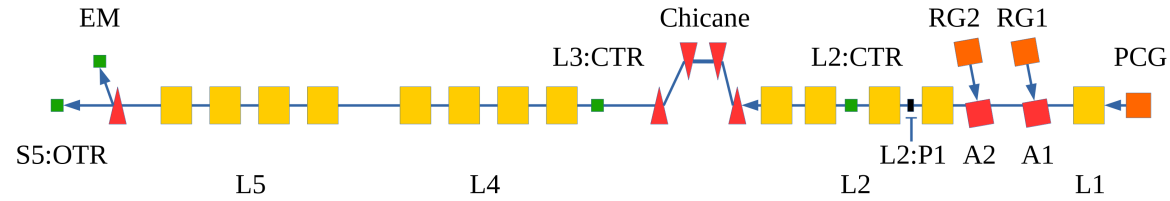

Figure 1: Linac schematic. The main accelerating sections are designated LX where X=1,2,4, and 5. Sections 2, 4, and 5 each have four 3-m SLEDed S-band accelerating structures. A1 and A2 are the alpha magnets associated with two TC rf gun beamlines RG1 and RG2. L2:P1 represents the BPM location for the macropulse measurements. L*:CM are current/charge monitors, ES is a spectrometer, triangles represent dipole magnets, and OTR images are collected at the S5:OTR station.

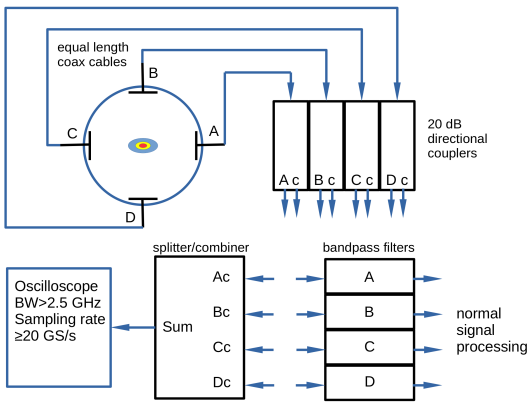

Figure 2: Macropulse measurement schematic.

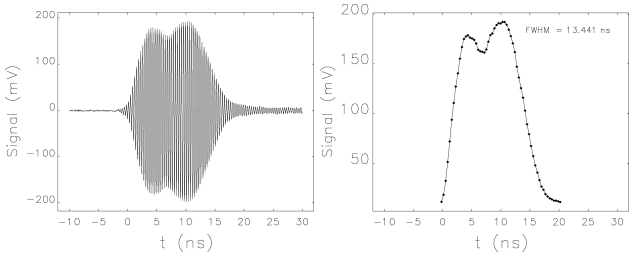

Figure 3: Left: Raw macropulse signal from the AET RG2 gun. Right: Peak detect envelope of the same signal.

gun will be conducted once accelerator operations resume in Fall 2023. Only the AET gun, installed in the RG2 location, was used in the bunch compression experiment discussed below.

MACROPULSE WAVEFORMS

An example of a raw macropulse waveform from one of the AET guns is plotted in Fig. 3, left. Figure 3, right shows the same signal after peak-detection processing to yield the envelope. This AET gun is located in the RG2 station; this is the gun beamline closest to the entrance of the linac known as the L2 section. A sampling rate, f_s of 20 GS/s provides 7 samples per fundamental rf period (350 ps) and yields a relatively smooth envelope after peak detection.

Macropulse data acquired for one of the new RadiaBeam guns is presented in Fig. 4. In this case, the gun is located in the RG1 station, approximately 3 m further from the L2

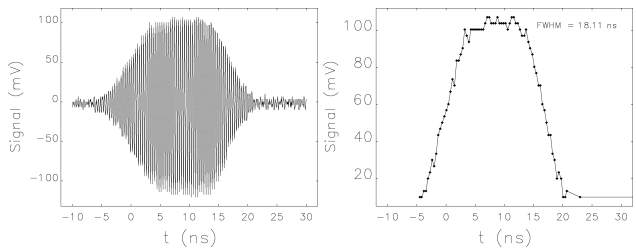

Figure 4: Left: Raw macropulse signal from the RG1 RadiaBeam gun. Right: Peak detect envelope of the same signal.

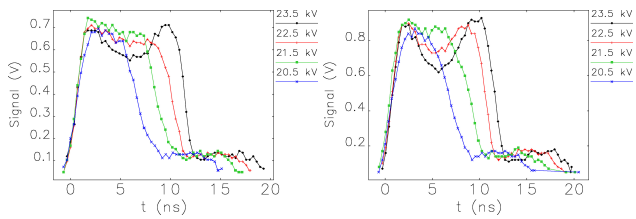

Figure 5: Macropulse envelope waveforms from the RG2 AET gun with varying chopper voltages for 190 mA (left) and 300 mA (right).

linac section than the RG2 gun. Transmission losses RG1 are typically higher than for RG2. Each station has its own chopper system; in the case of RG1 the chopper pulse is longer than that for RG2.

The macropulse waveforms were also observed as the chopper voltage as well as the average gun output current were varied. Waveforms at four chopper voltages are presented in Fig. 5 left and right for gun currents of 190 and 300 mA, respectively. Cathode heater power was varied to change the average gun current for the waveforms presented in Fig. 5. At higher voltages, we observed a double peak in the macropulse envelope. In this case, the beam is swept past the slit on the rising edge of the voltage pulse and again on the falling edge. Gun chopper voltage is the method used to control the charge per macropulse in the linac while the gun cathode heater power is typically maintained at a constant value. Macropulse duration varies from approximately 7 to 11 ns for both current levels as the chopper is raised from 20.5 to 23.5 kV. Current and charge data collected from current monitors in the linac during these measurements are presented in Table 1.

ISBN: 978-3-95450-236-3 ISSN: 2673-5350 doi:10.18429/JACoW-IBIC2023-TUP027

Table 1: RG2 Current and Charge Measurements

Chopper voltage (kV)	190 mA I_{CM} (mA)	190 mA Q_{CM2} (nC)	300 mA I_{CM} (mA)	300 mA Q_{CM2} (nC)
20.5	191	0.85	303	1.04
21.5	189	1.07	302	1.37
22.5	191	1.26	303	1.56
23.5	191	1.37	300	1.64

MICROPULSES AND MICROBUNCHING

The gun output current after the alpha magnet is modeled as a train of charge delta functions where each charge pulse is separated from its neighbor by one rf period. The current waveform may be expressed as,

$$I_g(t) = A(t)\delta\left(t - t_s - \frac{2\pi n}{\omega_{rf}}\right), \quad (1)$$

where $A(t)$ is the time-varying amplitude of the macropulse, t_s is time slip or jitter, δ is the delta function, and ω_{rf} is the radian frequency of RG2 rf drive power. The total charge is then determined integrating Eq. (1) over time,

$$Q = \int I_g(t)dt = \sum_n A\,(t_n) \quad (2)$$

where $t_n = t_s + 2\pi n/\omega_{rf}$. Respective calibration factors for the AET RG2 gun operating at currents of 190 mA and 300 mA are 56.33 ±0.97 pC/V and 55.36 ±1.49 pC/V; the maximum charge per micropulse at these currents are 39.99 ±0.88 pC and 49.88 ±1.66 pC.

For bunch compression studies, we are interested in the micropulse peak current. Compression studies were conducted with the RG2 AET TC gun beam. Two coherent transition radiation (CTR) interferometers are installed in the APS linac [8, 13]; one in the L2 section (L2CTR) between the second and third accelerating structures (AS), and another following the chicane in L3 (L3CTR), see Fig. 1. The four AS of L2 may be phased to chirp the pulses prior to the chicane to facilitate bunch compression. The beam energy after the L2 section was 150 MeV. The L2CTR sees the effect of the alpha magnet compression, whereas L3CTR observes compression provided by the chicane. Autocorrelations of the CTR signals at these two locations are presented in Fig. 6. Assuming a Gaussian profile for the compressed bunch, the rms bunch duration can be approximated as $\sqrt{2}\sigma_z/c$. For the autocorrelation scans shown in Fig. 6 this yields 300 fs and 130 fs from L2CTR and L3CTR, respectively. We assumed that the micropulse length is approximately constant over the macropulse duration. Using the FWHM duration, 50 pC results in a current of 170 A after the L3CTR. This current level is consistent with predictions made in Ref. [5].

During bunch-compression studies, gun output current was increased to 650 mA. Phasing the L2 AS to maximize compression, COTR was observed on the S5:OTR monitor, at an energy of 375 MeV [14]. Examples of OTR and

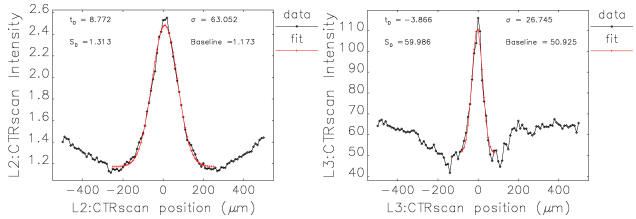

Figure 6: Autocorrelations of the coherent transition radiation signals from the L2CTR (left) and L3CTR (right) along with Gaussian fits to the central peak. RG2 (AET) source.

COTR emission are presented in Fig. 7. Emission intensity contour and profile data with L2 rf phased away from maximum compression are shown in the top row; the bottom row presents enhanced emission (COTR) at the maximum compression phase. The macropulse beam charge was monitored at L5:CM during data acquisition and was stable to less than 3 percent for both compressed and uncompressed measurements. The COTR/OTR intensity ratio is about 6.5 at the most enhanced spatial location. The two COTR-enhanced locations in the lower image (maximum compression) are approximately σ_x=380 μm by σ_y=50 μm in size. Compressed micropulse peak current was approximately 200 A.

Examining the effect of longitudinal space-charge (LSC) impedance, we plot in Fig. 8 Eq. (26) from Ref. [15] for R_{56} = 65 mm. With an rms energy spread of 2 keV, a gain of 5.7 is obtained at 800 nm. Signal intensity is proportional to the product of the COTR gain and the sensitivity of the CCD sensor integrated over the wavelength range of interest (400-1000 nm). Picking a COTR gain value in the red end of the range is meant to represent a rough estimate of the enhancement ratio. The gain is in reasonable agreement with the enhancement factor determined for the data plotted in Fig. 7. This is the first time a comparison has been done of empirical COTR gain from a TC rf gun source with an LSC impedance model.

Previous simulations of the LSC instability showed that microbunching in the visible wavelength regime can be supported if the slice energy spread of the microbunched portion of the beam is approximately 2-4 keV [16]. Using a PC rf gun source, an LCLS-I experiment generated COTR gain consistent with a slice energy spread of 3 keV. In the context of Ratner's LSC model, a 2 keV slice energy spread would be indicated to explain the observed COTR gain for the microbunched portion of the TC rf gun beam. This value is much smaller than the measured ensemble energy spread.

Broadband visible regime COTR enhancements have also recently been reported in laser-plasma-wakefield-accelerated beams [17–19], but this is a different microbunching mechanism. In this case, intense fields from a 100-TW-class drive laser interacting with the plasma electrons lead to microbunching.

SUMMARY

We described a method to measure the macropulse waveform of the APS TC rf guns. This method requires an oscillo-

ISBN: 978-3-95450-236-3 ISSN: 2673-5350 doi:10.18429/JACoW-IBIC2023-TUP027

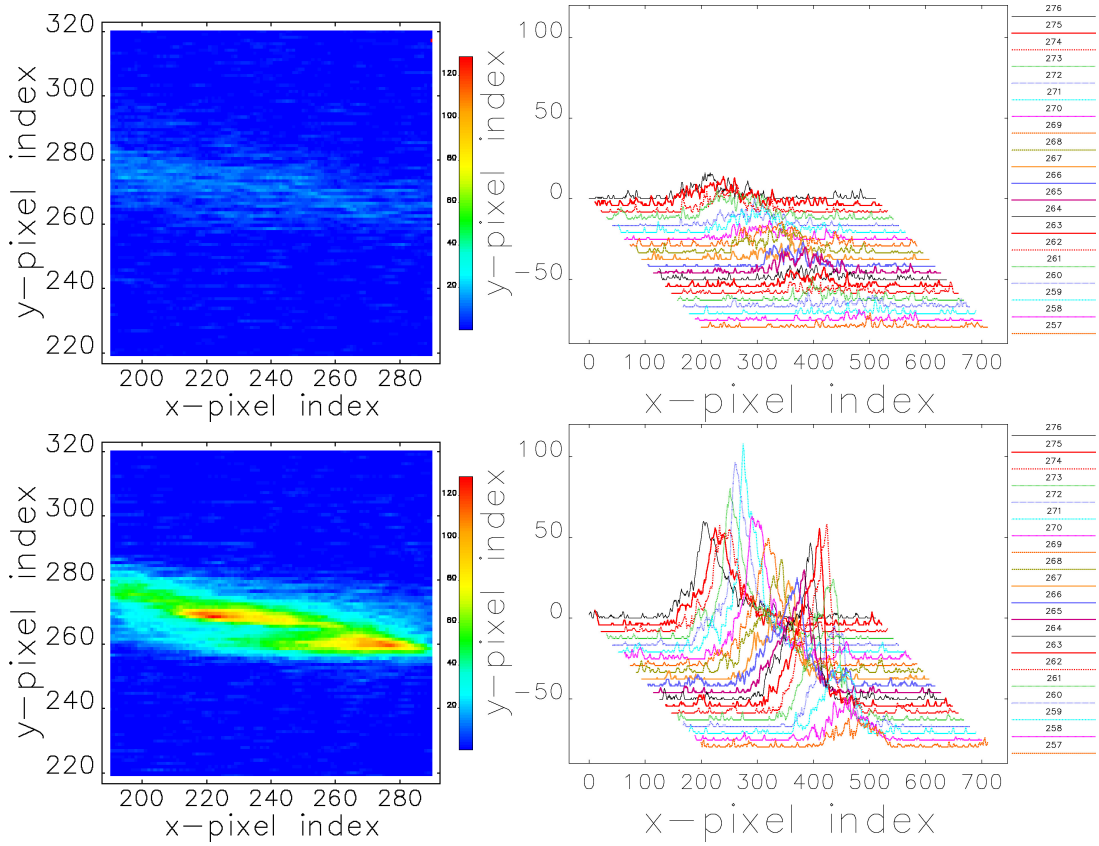

Figure 7: Top: Intensity contour plot (left) and line profiles (right) away from peak compression. Bottom: Intensity contour plot and line profiles near peak compression.

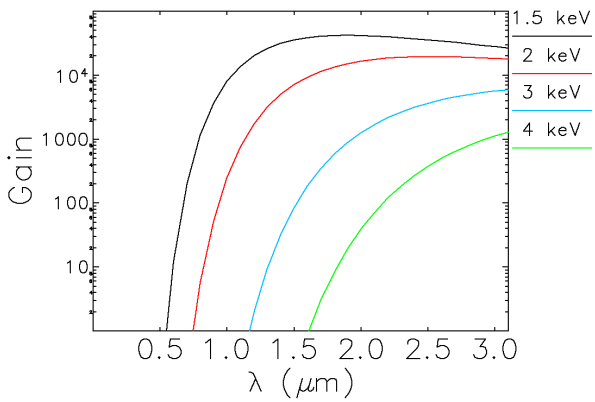

Figure 8: Microbunching gain as a function of wavelength for R_{56} = 65 mm with rms energy spread as a parameter.

scope with bandwidth and sampling rate sufficient to monitor the fundamental frequency of the rf applied to extract beam from the gun; in the present case, this requires a bandwidth > 2.5 GHz and sampling rate > 20 GS/s for 2865 MHz S-band rf. Measurement of the macropulse envelope allows for calibration of the microbunch charge and thereby calculation of peak currents after bunch compression. AET and RadiaBeam TC guns were tested and, accounting for differences in the chopper systems, behaved in a similar manner. Other methods employing diodes could be explored to eliminate the cost of an oscilloscope [20].

Additionally, we have inferred the presence of LSC-induced microbunching at visible wavelengths via the COTR mechanism from TC rf gun beams. After two stages of compression and with further acceleration to 375 MeV, an enhancement factor of 6.5 was observed in OTR near maximum compression. The enhanced emission is attributed to the generation of COTR from microbunching in the TC rf gun-generated micropulses. Analytical models indicate that a slice energy spread of only a few keV is needed for microbunching (COTR gain) at visible wavelengths where the CCD camera is sensitive. The importance of slice energy spread as it applies to a TC-rf gun-generated beam is analogous to what was reported for PC gun [16] and LPWA [17] beams. Further investigations including spectral measurements of the microbunching phenomena are warranted.

ACKNOWLEDGEMENTS

Thanks to R. Soliday and H. Shang for assistance with analysis scripts, of APS ANL.

REFERENCES

[1] K. J. Beczek, J. W. Lewellen, A. Nassiri, and E. Tanabe, "A Rationalized Approach to Thermionic RF Gun Design,"

ISBN: 978-3-95450-236-3 ISSN: 2673-5350 doi:10.18429/JACoW-IBIC2023-TUP027

in *Proc. PAC'01*, Chicago, IL, USA, Jun. 2001. https://jacow.org/p01/papers/WPAH052.pdf

[2] "Advanced Photon Source Upgrade Project Final Design Report," Advanced Photon Source, Argonne National Laboratory, Tech. Rep., 2019. https://publications.anl.gov/anlpubs/2019/07/153666.pdf

[3] S. V. Kutsaev *et al.*, "A New Thermionic RF Electron Gun for Synchrotron Light Sources," in *Proc. NAPAC'16*, Chicago, IL, USA, Oct. 2016, pp. 453–456. doi:10.18429/JACoW-NAPAC2016-TUB3CO04

[4] Y. W. Kang *et al.*, "Beam Chopper for the Low-Energy Undulator Test Line (LEUTL) in the APS," in *Proc. PAC'97*, Vancouver, Canada, May 1997, pp. 2699–2701.

[5] M. Borland, "A High-Brightness Thermionic Microwave Electron Gun," Available as SLAC Report 402, Ph.D. dissertation, Stanford University, 1991. https://www.slac.stanford.edu/pubs/slacreports/reports03/slac-r-402a.pdf

[6] M. Borland, "An Improved Thermionic Microwave Gun and Emittance-Preserving Transport Line," in *Proc. PAC'93*, Washington D.C., USA, Mar. 1993, pp. 3015–3018.

[7] J. W. Lewellen *et al.*, "Operation of the APS RF Gun," in *Proc. LINAC'98*, Chicago, IL, USA, Aug. 1998, pp. 863–865. https://jacow.org/l98/papers/TH4042.pdf

[8] A. H. Lumpkin, W. J. Berg, M. Borland, J. W. Lewellen, and N. S. Sereno, "Initial CTR-Based Bunch Length Measurements of Linac Beams Following the APS Bunch Compressor," in *Proc. FEL'03*, Tsukuba, Japan Sept. 2003, pp. 2420–2422. https://jacow.org/p03/PAPERS/WPPB005.pdf

[9] A. E. Grelick, "RF and Beam Diagnostic Instrumentation at the Advanced Proton Source (APS) Linear Accelerator," in *Proc. LINAC'96*, Geneva, Switzerland, Aug. 1996, pp. 851–853. https://jacow.org/l96/papers/THP75.pdf

[10] R. Lill, O. Singh, and N. Arnold, "New Beam Position Monitor System Design for the APS Injector," *AIP Conference Proceedings*, vol. 648, no. 1, pp. 401–408, 2002. doi:10.1063/1.1524426

[11] N. S. Sereno, M. Borland, and R. Lill, "Automated correction of phase errors in the advanced photon source linac," *Phys. Rev. ST Accel. Beams*, vol. 11, no. 7, p. 072 801, 2008. doi:10.1103/PhysRevSTAB.11.072801

[12] M. Wendt, "Direct (Under)Sampling vs Analog Downconversion for BPM Electronics," in *Proc. IBIC'14*, Monterey, CA, USA, Sep. 2014, pp. 486–494. https://jacow.org/IBIC2014/papers/WEIYB1.pdf

[13] A. Lumpkin, B. Yang, W. Berg, J. Lewellen, N. Sereno, and U. Happek, "Electron beam bunch length characterizations using incoherent and coherent transition radiation on the APS SASE FEL project," *Nucl. Instrum. Methods Phys. Res., Sect. A*, vol. 445, pp. 356–361, 2000.

[14] A. H. Lumpkin, "Beam Diagnostics for Coherent Optical Radiation Induced by the Microbunching Instability," in *Proc. FEL'13*, New York, NY, USA, Aug. 2013, pp. 169–172. https://jacow.org/FEL2013/papers/TUOBNO01.pdf

[15] E. Saldin, E. Schneidmiller, and M. Yurkov, "Klystron instability of a relativistic electron beam in a bunch compressor," *Nucl. Instrum. Methods Phys. Res., Sect. A*, vol. 490, pp. 1–8, 2002.

[16] D. F. Ratner, A. Chao, and Z. Huang, "Three-dimensional Analysis of Longitudinal Space Charge Microbunching Starting from Shot Noise," in *Proc. FEL'08*, Gyeongju, Korea, Aug. 2008, pp. 338–341. https://jacow.org/FEL2008/papers/TUPPH041.pdf

[17] C. Lin *et al.*, "Long-Range Persistence of Femtosecond Modulations on Laser-Plasma-Accelerated Electron Beams," *Phys. Rev. Lett.*, vol. 108, p. 094 801, 2012.

[18] A. H. Lumpkin *et al.*, "Coherent Optical Signatures of Electron Microbunching in Laser-Driven Plasma Accelerators," *Phys. Rev. Lett.*, vol. 125, p. 014 801, 2020. doi:10.1103/PhysRevLett.125.014801

[19] M. LaBerge *et al.*, "Coherent 3D Microstructure of Laser-Wakefield-Accelerated Electron Bunches," in *Proc. FEL'22*, 2022. doi:10.18429/JACoW-FEL2022-THAI2

[20] M. Gasior, "First Results from the LHC Schottky Monitor Operated with Direct Diode Detection," in *Proc. BIW'12*, Newport News, VA, USA, Apr. 2012, pp. 222–224. https://jacow.org/%20BIW2012/papers/TUPG044.pdf